China Petroleum Processing and Petrochemical Technology

Catalyst Research Volume 23, Issue 2, November 2023 Pp. 3217-3232

SOLUTE TRANSFER IN A PERMEABLE CHANNEL SUBJECT TO THE EFFECT OF VARIABLE VISCOSITY

P. Murali Mohan Kumar[1], M. Varunkumar[2]

[1]Department of Basic Sciences and Humanities, GMRIT Rajam-532 127. Andhra Pradesh, India.

[1]Department of Mathematics, School of Advance Sciences, VIT-AP University, Amaravati-522 237. Andhra Pradesh, India.

Abstract. This study presents a model for the solute transfer in fluid flow through a permeable channel with varying viscosity. An application of this model is to the flow of blood through glomerular capillaries. The amount of solute that can pass through the glomerular capillary wall is determined by the difference in pressure between the colloid osmotic pressure and the transcapillary hydrostatic pressure, as stated by Starling's rule. Analytical and numerical methods are used to solve the coupled equations controlling the fluid and solute transport. The results of this analysis are qualitatively in good agreement with those obtained from the experimental results. Based on the graphic representation of the data, it is obvious that varying viscosity affects velocity profiles, concentration profiles, as well as total clearance of solutes.

Keywords: Variable Viscosity; Starling's law; Glomerular capillary; Finite difference method; Ultrafiltration; Permeable wall

1. Introduction

The kidneys are responsible for excreting the bulk of human metabolism's end products and maintaining the concentrations of the majority of bodily fluid components, making them one of the most essential physiological organs. The major function of the kidney is to remove metabolic waste products from the body via urine. It is the job of the afferent arteriole to transport blood into the glomerulus, while the efferent arteriole is in charge of transporting blood away from the glomerulus. The vascular space and Bowman's capsule are free to exchange water and dissolved components during glomerular filtration. Starling's forces in the capillaries of glomerulus are what cause glomerular filtrate to develop. When these conditions are present, there is a fluid movement that is directed towards Bowman's capsule from the glomerular capillaries. Mathematical models have been constructed by a number of researchers in order to investigate the filtration mechanism in glomerular capillaries [1 - 6].

Brenner *et al.* [7, 8] examined on measures of mean and extravascular pressures in Bowman's space, solute concentration, and osmotic pressure at the extremities of the glomerulus, as well as GFR (glomerular filtration rate) of a single nephron. After conducting research into the connection between filtration and the increase in protein concentration brought on by ultrafiltration, Deen *et al.* [9] came to the realisation that the total ultrafiltration rate increases in proportion to the amount of blood that is being circulated through the body. By dropping the constant pressure gradient assumption, Marshal and Trowbridge [10] and Huss *et al.* [11] created models for glomerular ultrafiltration in which the intra-luminal pressure gradient was assumed to be dependent on the

Catalyst Research Volume 23, Issue 2, November 2023 Pp. 3217-3232

axial distance. Papenfuss and Gross [12] examined how the glomerular capillary wall's permeability and pressure drop affected the filtration process.

The researchers of the above mentioned literature have not taken into account solute transport across the capillary membrane. Salathe [13] investigated solute transport across the capillary wall under the presumption that the concentration was constant throughout. Deen et al. [14] discovered that the glomerular filtration rate is extremely sensitive to changes in glomerular blood flow during filtration pressure equilibrium. They also showed that the osmotic pressure profile along the glomerular capillary is nonlinear. By assuming zero osmotic pressure, Ross [15] developed a model for mass transfer through a permeable tube with a modest radial flux of fluid. For the scenario of combination dialysis and filtration, Tyagi and Abbass [16] provided an analytical solution for a steady solute distribution when blood flows through a hollow-fibre artificial kidney. Both hydrostatic and osmotic pressure affect filtration velocity and protein transfer inside and over the capillary wall (Chaturani and Ranganatha [17]). Varunkumar and Muthu ([18, 19]) developed a solution for solute transport in a porous capillary with changeable-permeability, slip coefficient, osmotic pressure along the porous wall based on solute concentration. The model described by Nazarenko [20] took into account the expansion of concentrations, compressibility, and also the friction within a porous cylindrical layer.

According to the preceding review of the literature, there has never been a study of fluid and solute transfer with variable viscosity, as well as the presence of concentration dependency of osmotic pressure so far. Examining solute movement in a channel with a permeable boundary and variable viscosity is the main goal of this research [21, 22]. Davis and Sherwood [23] investigated the effect of the varying viscosity and diffusivity by taking mass transfer eauation in a steady-state boundary layer. Bowen and Williams [24] studied cross-flow ultrafiltration for concentration-dependent viscosity and diffusivity. Shamsuddin *et al.* [25] investigated concentration polarization as a coupled transport problem with concentration-dependent solute viscosity and developed a thorough good understanding of the influence of viscosity changes on solute concentration. According to the preceding review of the literature, there has never been a study of fluid flow and solute transport via permeable channel with varying viscosity, as well as the presence of concentration dependency of osmotic pressure so far. Analytical and numerical approaches are used to solve the flow equations, while an implicit finite difference technique is used to solve the solute transport equation. With the use of graphical findings, the profiles of hydrostatic, osmotic, velocity, and concentration distributions for the emerging parameters are illustrated and analyzed in detail. The mathematical model and the details of solution methodology are given below.

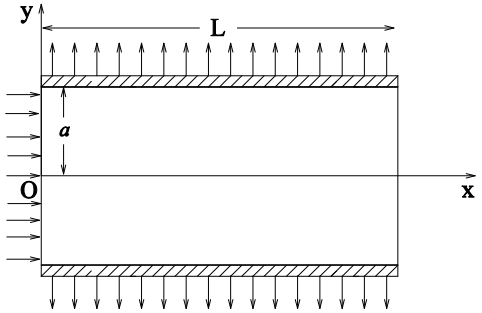

Catalyst Research Volume 23, Issue 2, November 2023 Pp. 3217-3232

Figure 1: Geometrical model of the glomerular capillary.

2. Formulation of the problem

Consider the steady incompressible Newtonian fluid and solute transfer in a permeable channel of length L and half width a (see Figure 1). Figure 1 depicts the channel's coordinate system, which includes the axial and transverse directions $\hat{x}$ and $\hat{y}$, respectively. The equations that control fluid flow with varying viscosity $\hat{\mu}(\hat{y})$, as indicated by the fluid's continuity and momentum,

$$\frac{\partial \hat{u}}{\partial \hat{x}} + \frac{\partial \hat{v}}{\partial \hat{y}} = 0 \tag{1}$$

$$\rho\left(\hat{u}\frac{\partial \hat{u}}{\partial \hat{x}} + \hat{v}\frac{\partial \hat{u}}{\partial \hat{y}}\right) = -\frac{\partial \hat{p}}{\partial \hat{x}} + 2\frac{\partial}{\partial \hat{x}}\left(\hat{\mu}(\hat{y})\frac{\partial \hat{u}}{\partial \hat{x}}\right) + \frac{\partial}{\partial \hat{y}}\left(\hat{\mu}(\hat{y})\left(\frac{\partial \hat{u}}{\partial \hat{y}} + \frac{\partial \hat{v}}{\partial \hat{x}}\right)\right) \tag{2}$$

$$\rho\left(\hat{u}\frac{\partial \hat{v}}{\partial \hat{x}} + \hat{v}\frac{\partial \hat{v}}{\partial \hat{y}}\right) = -\frac{\partial \hat{p}}{\partial \hat{y}} + 2\frac{\partial}{\partial \hat{y}}\left(\hat{\mu}(\hat{y})\frac{\partial \hat{u}}{\partial \hat{y}}\right) + \frac{\partial}{\partial \hat{x}}\left(\hat{\mu}(\hat{y})\left(\frac{\partial \hat{u}}{\partial \hat{y}} + \frac{\partial \hat{v}}{\partial \hat{x}}\right)\right) \tag{3}$$

The solute transfer in such system is,

$$\hat{u}\frac{\partial \hat{c}}{\partial \hat{x}} + \hat{v}\frac{\partial \hat{c}}{\partial \hat{y}} = D\left(\frac{\partial^2 \hat{c}}{\partial \hat{x}^2} + \frac{\partial^2 \hat{c}}{\partial \hat{y}^2}\right) \tag{4}$$

where, the axial, transverse velocities, concentration of solute and pressure are represented by $\hat{u}(\hat{x},\hat{y})$, $\hat{v}(\hat{x},\hat{y})$, $\hat{c}(\hat{x},\hat{y})$ and $\hat{p}$, respectively. Here $\rho$is the density and $D$is the diffusion-coefficient.

The following are the velocity and concentration boundary conditions for the current problem:

At $\hat{y} = 0$ (Symmetric condition),

$$\frac{\partial \hat{u}}{\partial \hat{y}} = \frac{\partial \hat{c}}{\partial \hat{y}} = \hat{v} = 0 \tag{5}$$

At $\hat{y} = a$,

$$\hat{v} = k(\Delta\hat{P} - \sigma\Delta\hat{\pi}) = V_a \tag{6}$$

$$\hat{u} = 0 \tag{7}$$

$$-D\frac{\partial \hat{c}}{\partial \hat{y}} = h(\hat{c} - c_T) + (T_a - 1)V_a\Phi \tag{8}$$

where$\Phi = \begin{cases} \hat{c}; & V_a > 0 \\ c_T; & V_a < 0 \end{cases}$. The no-slip condition is the equation (7) and the solute mass flow equation is represented by (8) [28].

At $\hat{x} = 0$,

$$\hat{c} = c_0 \tag{9}$$

$$\Delta\hat{P} = \Delta P_a \tag{10}$$

$$\int_0^a \hat{u}\,(0,\hat{y})d\hat{y} = Q_0 \tag{11}$$

The first condition is a uniformly distributed solute concentration, the second is constant hydrostatic pressure, and the third condition is constant flow at $x = 0$. $\Delta\hat{P} = \hat{P} - P_T$, $\Delta P_a = P_a - P_T$, $\Delta\hat{\pi} = \hat{\pi} - \pi_T$, $\hat{P}$ and P_T denote the hydrostatic pressures within and outside of the channel wall, respectively. $\hat{\pi}$ and π_T are the osmotic pressures within and outside of the wall, respectively. P_a and Q_0 denote the hydrostatic pressure and volume flow rate, respectively, at the beginning of

Catalyst Research Volume 23, Issue 2, November 2023 Pp. 3217-3232

the channel. The hydraulic permeability of the wall is denoted by k, the reflection coefficient is denoted by σ. In this case, $c_0$and c_T stand for the concentration of the solute at the entrance of the channel and the concentration outside the channel, respectively. P_T and π_T are taken to be constants in this calculation. Meanwhile, h stands for the solute permeability, and T_a stands for the transmittance coefficient. The osmotic pressure can be expressed as a function of the concentration of a solute [12],

$$\hat{\pi}(\hat{x}) = 0.009\,\hat{c}^3 + 0.16\,\hat{c}^2 + 2.1\,\hat{c} \quad (12)$$

The solute mass flux (J_s) and total solute clearance (J_{cl}) over the permeable channel wall,

$$\hat{J}_s(\hat{x}) = h(\hat{c}(\hat{x},a) - c_T) + T_a V_a \Phi, \quad \hat{J}_{cl} = a\int_{\hat{x}=0}^{\hat{x}=L} \hat{J}_s(\hat{x})\,d\hat{x} \quad (13)\text{-}(14)$$

Following is a list of the non-dimensional quantities that are introduced:

We non-dimensionalise the equations by defining: $x = \hat{x}a$, $y = \hat{y}a$, $u = \hat{u}U_0$, $v = \hat{v}U_0$, $V_a = \widehat{V_a}U_0$, $c = \hat{c}c_0$, $c_T = \widehat{c_T}c_0$, $\Delta\pi = \Delta\hat{\pi}\Delta P_a, \Delta P = \Delta\hat{P}\Delta P_a$, $b_1 = \hat{b}_1\Delta P_a/c_0$, $b_2 = \hat{b}_2\Delta P_a/c_0^2$, $b_3 = \hat{b}_3\Delta P_a/c_0^3$, $J_s = \widehat{J_s}c_0 D/a$, $J_{cl} = Q_0 c_0\widehat{J_{cl}}$, $Q = Q_0\hat{Q}$, $\mu = \mu_0\hat{\mu}$,

Axial diffusion in glomerular capillaries is less effective than radial diffusion [16]. Due to the fact that the ratio of the channel length to the half width is expected to be quite high, there are no end effects. In addition, it is possible to disregard the effects of inertia due to the fact that the net radial flow is relatively modest in contrast to the average axial flow (Reynolds number is of the order 0.001). When these non-dimensional quantities and assumptions are included, the governing equations and boundary conditions are rewritten to reflect the new form (after dropping hats),

$$\frac{\partial u}{\partial x} + \frac{\partial v}{\partial y} = 0, \quad (15)$$

$$a_p\frac{\partial(\Delta P)}{\partial x} = \frac{\partial}{\partial y}\left(\mu(y)\frac{\partial u}{\partial y}\right), \quad (16)$$

$$\frac{\partial(\Delta P)}{\partial y} = 0, \quad (17)$$

$$u\frac{\partial c}{\partial x} + v\frac{\partial c}{\partial y} = \frac{1}{Pe}\frac{\partial^2 c}{\partial y^2} \quad (18)$$

At $y = 0$,

$$\frac{\partial u}{\partial y} = \frac{\partial c}{\partial y} = v = 0 \quad (19)$$

$$v = \varepsilon a_p(\Delta P - \sigma\Delta\pi) = V_a, \quad (20)$$

$$u = 0 \quad (21)$$

$$\frac{\partial c}{\partial y} = Sh_w(c_T - c) + Pe(1 - T_a)V_a\Phi \quad (22)$$

At $x = 0$,

$$c = 1, \quad \Delta P = 1, \quad \int_0^1 u(0,y)dy = 1 \quad (23\text{-}25)$$

Equations (13) and (14) are presented in their non-dimensional form as,

$$J_s = Sh_w(c(x,1) - c_T) + PeT_aV_a\Phi\,, J_{cl} = \frac{1}{Pe}\int_0^{L/a} J_s\,dx, \quad (26)\text{-}(27)$$

Catalyst Research Volume 23, Issue 2, November 2023 Pp. 3217-3232

where, $\varepsilon = k\mu_0/a$, $Pe = U_0 a/D$, and $Sh_w = ha/D$ are ultrafiltration parameter, Peclet number and Sherwood number, respectively.

3. Solution of the Problem

The equations (15) and (16) with (19) and (21) give the velocities $u(x,y)$ and $v(x,y)$ as,

$$u(x,y) = -a_p \frac{d(\Delta P)}{dx} \int_y^1 \frac{y}{\mu(y)} dy \tag{28}$$

$$v(x,y) = a_p \frac{d^2(\Delta P)}{dx^2} \left(y \int_y^1 \frac{y}{\mu(y)} dy + \int_0^y \frac{y^2}{\mu(y)} dy \right). \tag{29}$$

The equation (29) and the boundary condition (20) determine the second order ODE for the hydrostatic pressure,

$$\frac{d^2(\Delta P)}{dx^2} - \frac{\varepsilon(\Delta P - \sigma \Delta \pi)}{I_1} = 0. \tag{30}$$

The equations (24) and (25) are written in the following way: At $x = 0$,

$$\Delta P = 1 \tag{31}$$

$$\frac{d\Delta P}{dz} = -\frac{1}{a_p I_2} \tag{32}$$

The osmotic pressure difference in non-dimensional form as,

$$\Delta\pi = \pi - \pi_T = 2.1[c(x,1) - c_T] + 0.16[c(x,1)^2 - c_T^2] + 0.009[c(x,1)^3 - c_T^3]. \tag{33}$$

where $I_1 = \int_0^1 \frac{y^2}{\mu(y)} dy$ and $I_2 = \int_0^1 \int_y^1 \frac{y}{\mu(y)} dy dy$.

Integrations in the equations (28)-(29) and (30)-(32) are impacted by the viscosity of the fluid. In this inquiry, the exponential viscosity model is applied, and its equation can be stated as follows:

$$\mu(y) = e^{-\alpha} \tag{35}$$

where α is the viscosity parameter. All the computations have been done with exponential form of viscosity. The equations (28) and (29) give the axial and transverse velocities, which are in terms of $c$and ΔP. The solutions of the equations (18) and (30), for solute concentration (c) and hydrostatic pressure (ΔP) are difficult to obtain analytically, due to the coupling of equations. Therefore, the equations (18) and (30) are solved by using numerical techniques(RK-4 method and Finite difference method) with boundary conditions (19, 22, 23) and (31, 32) respectively.

4. Numerical Technique

To solve the solute transport equation (18) with the beginning and boundary conditions, Crank-Nicolson type finite difference technique was employed (19, 22, 23). Varun and Muthu [18] both provided comprehensive explanations of the solution technique. To validate the numerical approach, the grid independence test is performed. Hydrostatic pressure distributions in the axial direction were observed for various grid points in the transverse direction. The step size is set in one direction and may be varied in another with values of $0.1, 0.2, 0.3,$ and 0.4. 51×11, 51×21, 51×31, and 51×41 different nodes are generated by the four runs, respectively. For each of these instances, a C++ program is compiled. After experimenting with a few different mesh sizes, the mesh size 51×11 was found to be the most accurate in predicting

flow physics, and it was utilized in this study. Only the fifth decimal place separates the two sets of results. As a result, these mesh sizes are thought to be suitable for the computations at hand. In the finite-difference approximation, the truncation error is $O(\Delta y^2 + \Delta x)$ and approaches to zero as $\Delta y,\ \Delta x \to 0$. As a result, the system works. Varun and Muthu [18] demonstrated how the finite difference scheme is always stable. Convergence is ensured through consistency and compatibility.

5. Results and Discussions

Fluid and solute transport through a permeable channel has been studied using a mathematical model of variable viscosity in the glomerular capillaryThe computational results are attained for a collection of physiologically significant factors [12, 17]. The graphs show the impacts of variable viscosity and other developing factors on pressure, velocities, solute concentration, and total solute clearance.

6. Hydrostatic and Osmotic Pressures

For various values of the viscosity parameter (α) and other emergent parameters, the distributions of hydrostatic and osmotic pressure profiles with respect to axial distance are shown in Figures 2 - 5. These distributions are shown for a range of axial distances. Both the hydrostatic and osmotic pressure curves agree quite well with the data from the experiments [27]. The difference in pressure, denoted by ΔP, decreases in a linear fashion while the osmotic pressure $(\Delta\pi)$ enhances in a non-linear manner along the capillary axial length. Figure 2 depicts the effect of the viscosity parameter (α) on hydrostatic (Δp) and osmotic pressure $(\Delta\pi)$. The value of ΔP rises all the way along the axial length whenever the parameter α is increased. This suggests that a higher pressure is required for driving fluids that have a greater viscosity (see (Fig. 2(a)). The values of the osmotic pressure, denoted by $\Delta\pi$, are shown to decrease when it is shown that the parameter(α), is increased (Fig. 2(a)). This was found to be consistent with what was predicted in [29].

The ΔP profiles are unaffected by the solute wall permeability h and the transmittance coefficient T_a, as shown in Figure 3. As T_a and h, the osmotic pressure decreases along the axial length, indicating that the solute has passed through the channel wall. Refer to Fig. 4(a) to see how the osmotic pressure $(\Delta\pi)$ rises as the input pressure (ΔP_a) rises. The increase in T_a values indicates that there is more solute transport over the capillary wall, and as a result, osmotic pressure drops in the x −direction (Fig. 4(b)). The influence of initial average velocity (U_0) on hydrostatic pressure and osmotic pressure is seen in Fig. 5. As U_0 grows, ΔP drops in the axial direction (Fig. 5(a)). $\Delta\pi$ diminishes as U_0 grows (see Fig. 5(b)).

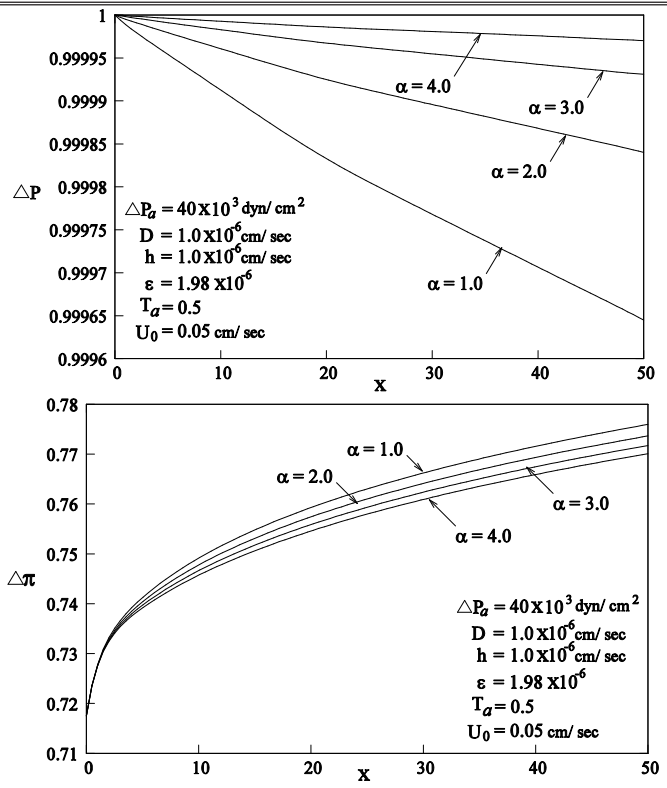

(a) (b)

Figure 2: Distribution of ΔP and $\Delta\pi$ for different α values.

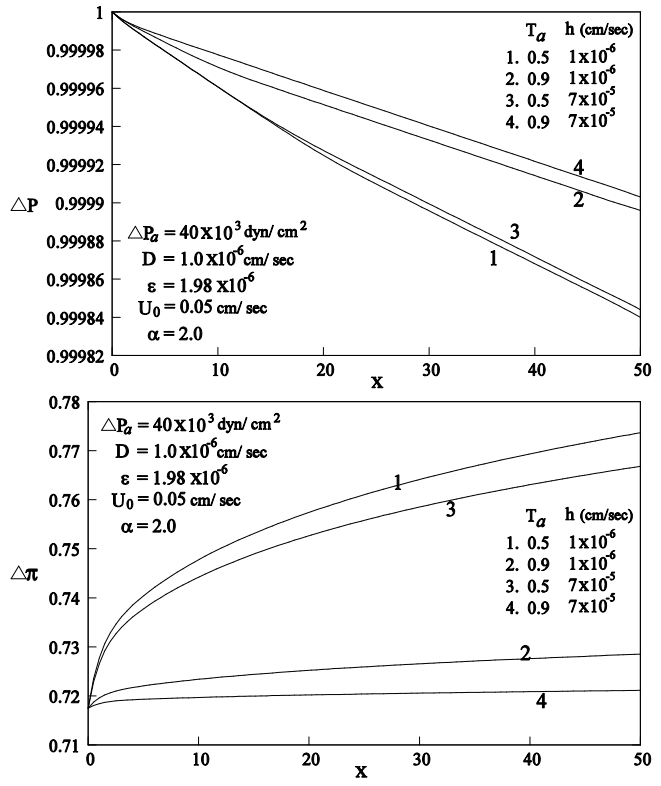

(a) (b)

Catalyst Research Volume 23, Issue 2, November 2023 Pp. 3217-3232

Figure 3: Distribution of hydrostatic and osmotic pressures for different T_a and $\boldsymbol{h}$.

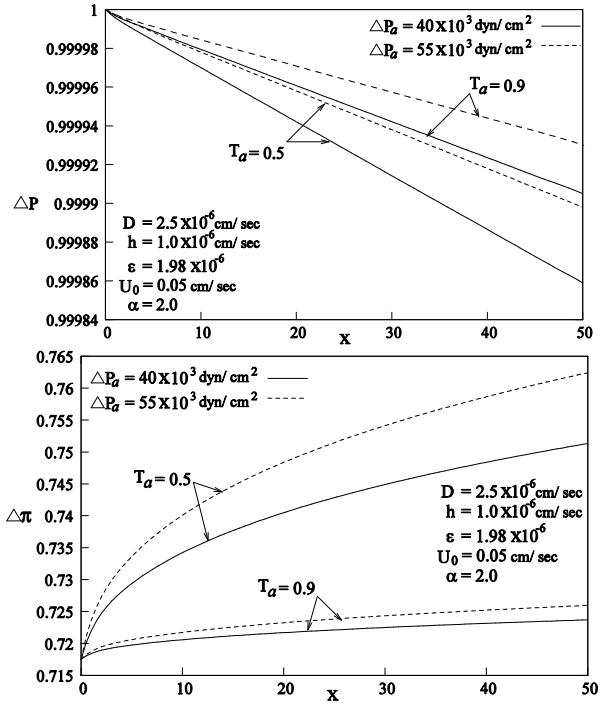

(a) (b)

Figure 4: Distribution of hydrostatic and osmotic pressures for different $T_a$and ΔP_a

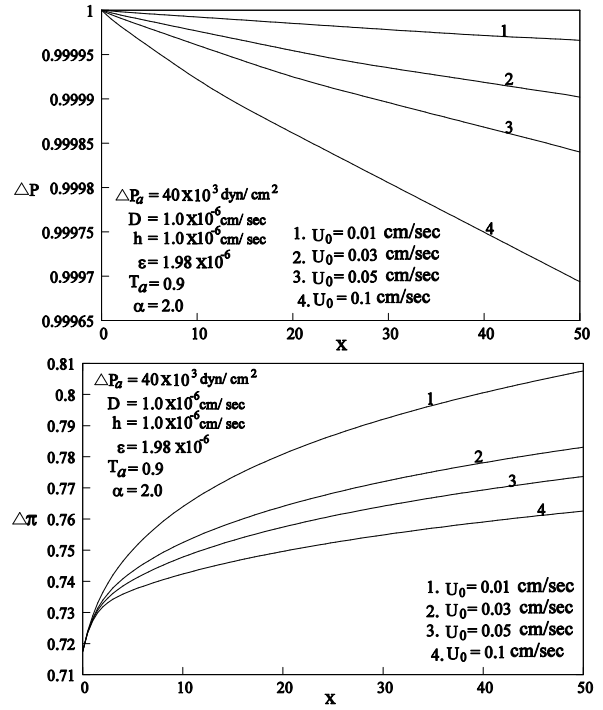

(a) (b)

Figure 5: Distribution of hydrostatic and osmotic pressures for different U_0.

Catalyst Research Volume 23, Issue 2, November 2023 Pp. 3217-3232

7. Axial Velocity $(u(x,y))$ and Transverse Velocity $(v(x,y))$

At different axial positions, figure 7 depicts the behavior of the axial velocity u with y for various α values. Along the length of the capillary, the axial velocity (u) is found to decrease. As the parameter α varies, the axial velocity near the channel axis decreases. Figure 8 depicts the effects of the viscosity parameter (α) on transverse velocity (v) at various points along the channel. When the parameter α is increased, the transverse velocity rises at the boundary but drops near the end of the channel. That is, at the position $x = 15$, the transverse velocity is greater than at the channel's end, $x = 50$. It is worth noting that the viscosity parameter (α) has a significant influence on flow behavior. As the varying viscosity $\mu(y) \to 1$, which gives the constant viscosity case [17], the estimated $u -$ and $v -$velocity values match well.

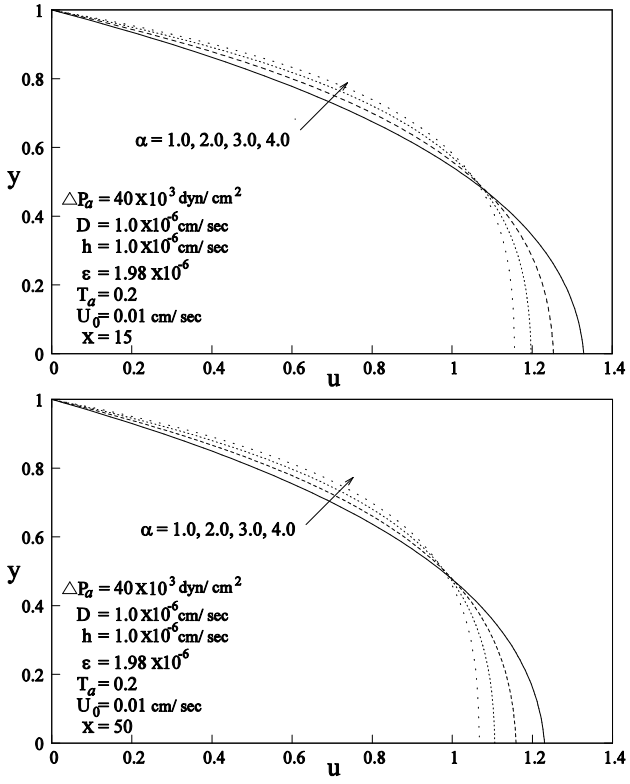

(a) (b)

Figure 6: Distribution of axial velocity at different cross-sections along the axis for variousαvalues.

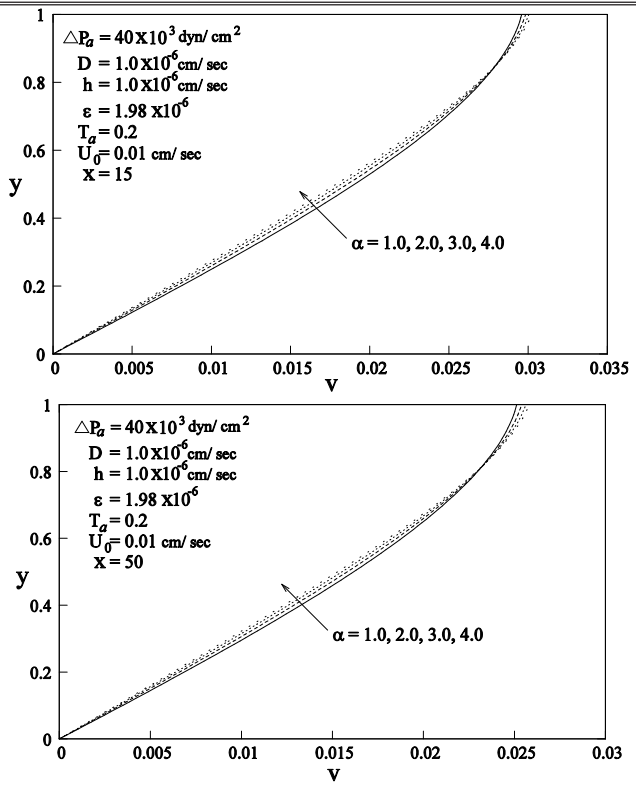

(a) (b)

Figure 7: Distribution of transverse velocity at different cross-sections along the axis for various α values.

8. Concentration Profiles $c(x, y)$

The influence of the viscosity variation on solute concentration at different locations is depicted in the figure 8. When α increases, there is a negligible increase in the concentration at the centerline, but there is a decrease in the concentration close to the wall. The solute concentration rises toward the wall, where it achieves its highest value. The solute concentration rises toward the wall. The distribution of solute concentrations along the length of the channel is depicted in figure 9, which illustrates the results for two different sites at varying T_a and h. Because c has a bigger value at the wall, the significance of any position along the axis is greater than that of a point on the wall. This takes place as a result of the equilibrium that is struck between convection toward the wall and the diffusion away from it. Because ultrafiltration removes the solutes, the concentration of solutes rises with increasing transverse distance at any given channel cross-section.

Figure 10 displays the impact that ε and D have had on the distribution of the concentrations. The concentration of the solute increases as the value of ε increases, indicating that the volume of the solute per unit volume at the wall has increased. When D increases, the concentration of solutes along the axis drops, as shown above. It is correct to say that when $\varepsilon = 0$, there is no solute movement through the wall since there is no permeability (zero ultrafiltration). This indicates that the transversal concentration profile reaches zero at the cross-section shown by the value $x = 15$, having dropped significantly from the starting constant value $c_0 = 1$.

Catalyst Research Volume 23, Issue 2, November 2023 Pp. 3217-3232

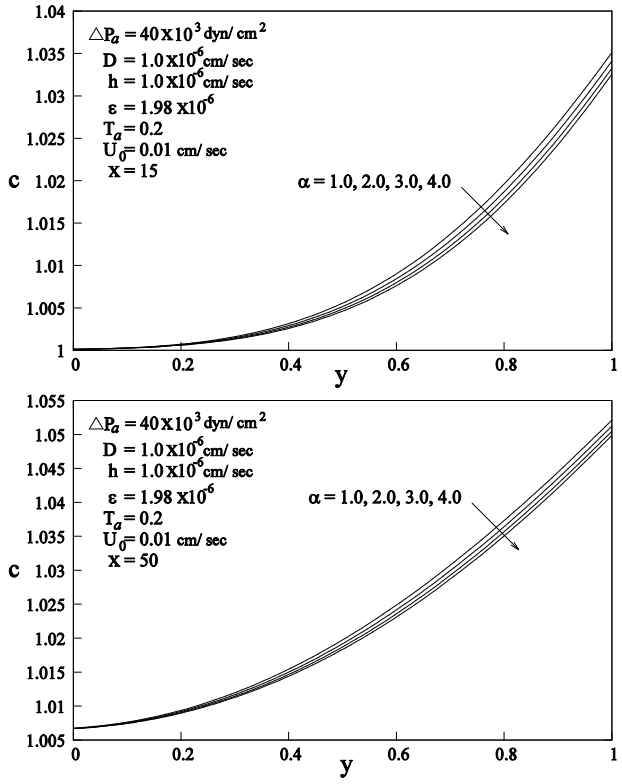

(a) (b)

Figure 8: Distribution of solute concentration for different values of α with $y$at different axial positions.

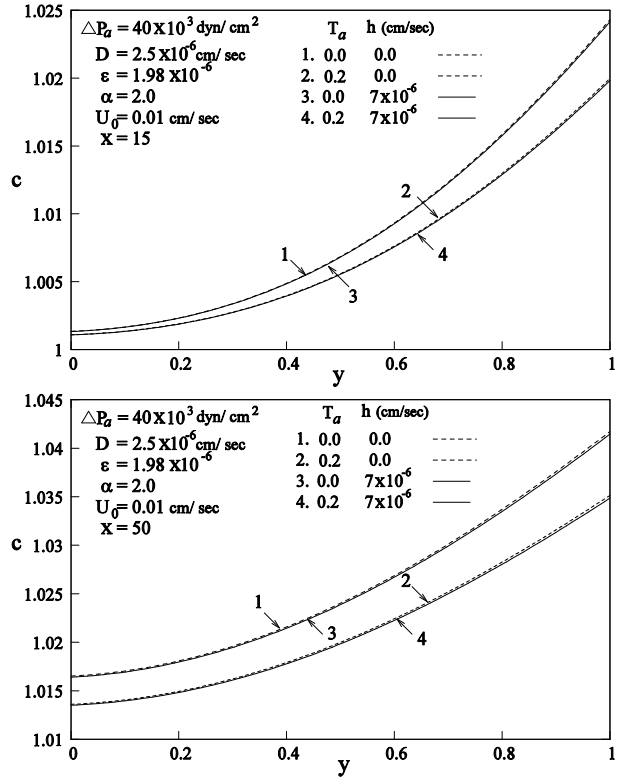

(a) (b)

Figure 9: Distribution of solute concentration for different T_a and h values with $y$at different axial positions.

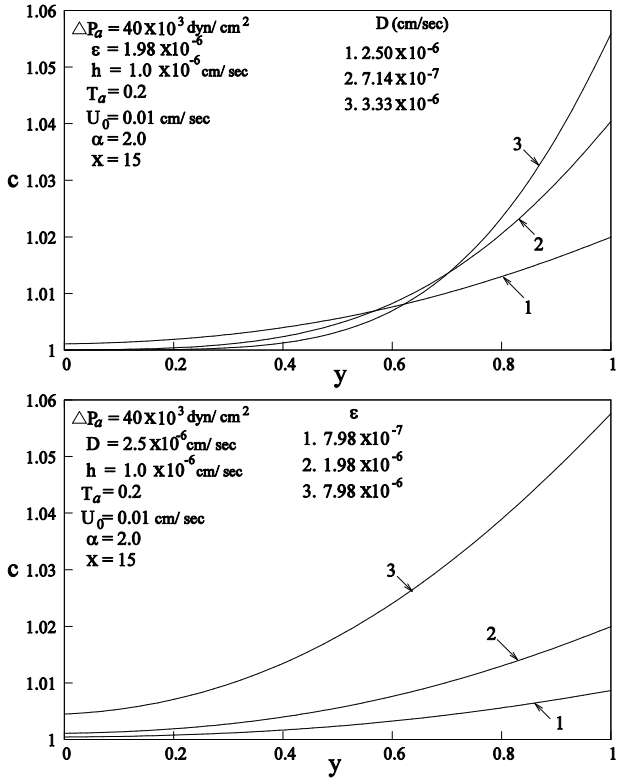

(a) (b)

Figure 10: Distribution of solute concentration for different ε and D values.

9. Wall concentration c_w

Figure 11 shows how the viscosity parameter (α) affects the value concentration c_w. It should be noticed that concentration varies only along the porous wall. The concentration close to the wall decreases as α rises, which is also important to note. Figure 12(a) shows the distribution of c_w for various T_a and h values. In determining the concentration of solutes on the walls, transmittance coefficients and wall permeability values play a crucial role. That is, as T_a and h grow, the c_w decreases. Figure (12) depicts the wall concentration (c_w) as a function of axial length for different ultrafiltration parameter (ε). As ε grows, so does the concentration at the wall (c_w). In this investigation, it is said that osmotic pressure and ultrafiltration have a bigger influence than hydrostatic pressure.

Catalyst Research Volume 23, Issue 2, November 2023 Pp. 3217-3232

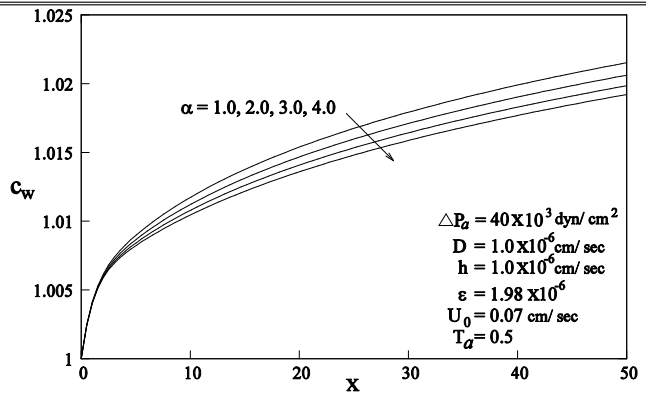

Figure 11: Distribution of solute wall concentration for different α values.

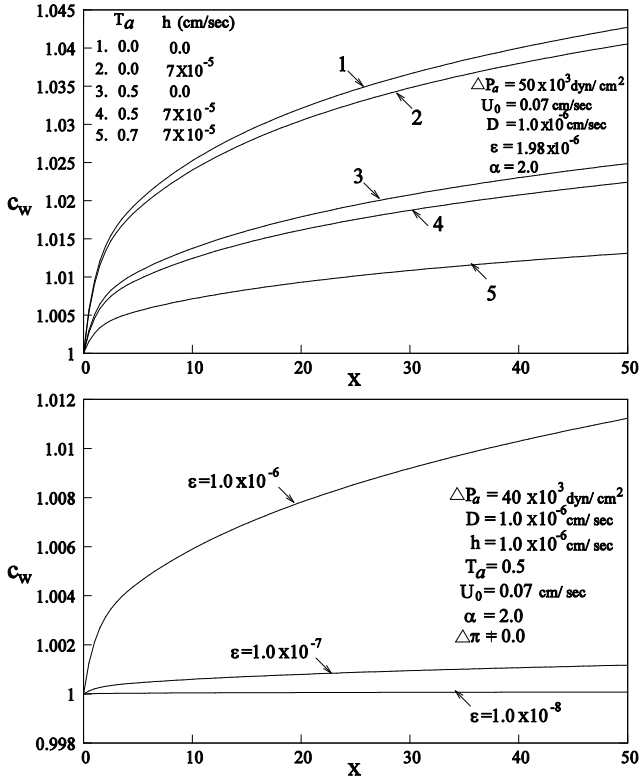

(a) (b)

Figure 12: Distribution of solute concentration for different (a) T_a and h and (b) ε values.

10. Total solute clearance(J_{cl})

Table I discusses the findings of total solute clearance (J_{cl}) with varying viscosity. The current model uses a range of α from 1.0 to 4.0. The values of the other parameters are within the physiological data ranges. It is observed that as α rises, the total solute clearance increases, as do h, and ε.

Table 1. J_{cl} for $U_0 = 0.07\ cm/sec, T_a = 0.5, \Delta P_a = 40 \times 10^3 dyn/cm^2$ and $D = 1 \times 10^{-6} cm^2/sec$

	$\varepsilon = 7.98 \times 10^{-7}$	$\varepsilon = 1.98 \times 10^{-6}$

Catalyst Research Volume 23, Issue 2, November 2023 Pp. 3217-3232

α	$Sh = 0.005$	$Sh = 0.035$	$Sh = 0.005$	$Sh = 0.035$
1.0	0.0535265	0.0674575	0.119826	0.135206
2.0	0.0536864	0.0675728	0.120648	0.135919
3.0	0.0538081	0.0676582	0.121299	0.136481
4.0	0.0539036	0.067724	0.121822	0.136933

11. Conclusions

To our knowledge, the model provided in this paper is the first mathematical model of fluid and solute transport in glomerular capillaries that takes into consideration varying viscosity and permeability properties. Novel components of the study include the investigation of solute transfer via a permeable channel, as well as the application of changing viscosity, particularly to the solute movement in glomerular capillaries. In order to solve the coupled equations governing the fluid movement and solute concentration, numerical solutions were developed. For the purpose of solving the solute transfer equation, the implicit Crank-Nicolson technique is applied. In this study, the effects of changing viscosity on profiles of hydrostatic and osmotic pressures, velocity, solute concentration, and the total solute clearance were examined.

- As viscosity parameter α, is decreased, the hydrostatic pressure increases linearly over the entire axial length of the channel. The osmotic pressure curves rise in an exponential rather than linear fashion as the axial distance increases. As the value of α increases, the value of $\Delta\pi$ will decrease.
- The values of the axial and transverse velocities at the boundary increase as α increases.
- With increasing viscosity, the concentration at the axis rises while it falls at the wall.
- As the viscosity parameter is decays, the wall concentration increases. The discrepancy between the two outcomes grows as viscosity parameter ε rises.
- With increasing values of α, h, and ε, the total solute clearance $(\boldsymbol{J_{cl}})$ rises.

It should be emphasized that the current model depicts mass transport in a channel with uniform walls. However, capillaries are not uniform in real-life physiological conditions. As a result, by expanding the above study to a non-uniform channel or tube, this model may be made more realistic

Author Contributions

P. Murali Mohan Kumar formulated the concept, began the work, and proposed the model; M. Varunkumar carried out the approach and looked at the manuscript's theoretical justification; A. S . V. analyzed the findings; and all the authors discussed, reviewed, and gave their approval to the manuscript's final document.

References

[1] Berman, A. S., Laminar flow in an annulus with porous walls, *Journal of Applied Physics,* 29, 1958, 71-75.

[2] Apelblat, A., Katchasky, A. K. and Silberberg. A, A mathematical analysis of capillary tissue fluid exchange, *Biorheology*, 11, 1974, 1-49.

[3] Palatt, J. P., Henry S. and Roger I. T., A hydrodynamical model of a permeable tubule, *Journal of theoretical Biology*, 44, 1974, 287-303.

[4] Guyton, A. C. and John. E. H., *Text Book of Medical Physiology*, 11th Edition, Elsevier Saunders Publishing, 2011.

[5] James Keener and James Sneyd, *Mathematical Physiology*, 2nd Edition, Springer, 2009.

[6] Vander, A. J., Sherman, J. H. and Luciano, D. S., *Human Physiology-The mechanisms of body function*, 2nd Edition, TMH, New Delhi, 1975.

[7] Brenner, B. M., Troy, J. L., Daugharty, T. M. and Deen, W. M., Dynamics of glomerular ultrafiltration in the rat. II. Plasma flow dependence of GFR. *American Journal of Physiology,* 223, 1972, 1184-1190.

[8] Brenner, B. M., Baylis, C. and Deen, W. M., Transport of molecules across renal glomerular capillaries, *Physiol. Rev.,* 56, 1978, 502-534.

[9] Deen, W. M., Robertson, C. R. and Brenner, B. M., A model of glomerular ultrafiltration in the rat. *American Journal of Physiology*, 223, 1972, 1178-1183.

[10] Marshall, E. A. and Trowbridge, E. A., A mathematical model of the ultrafiltration process in a single glomerular capillary, *Journal of theoretical Biology*, 48, 1974, 89- 412.

[11] Huss, R. E., Marsh, D. J., and Kalaba, R. E., Two models of glomerular filtration rate and renal blood flow in the rat, *Annals of Biomedical Engineering*, 3, 1975, 72-99.

[12] Papenfuss, H. D. and Gross J. F., Analytical study of the influence of capillary pressure drop and permeability on glomerular ultrafiltration, *Microvascular Research*, 16, 1978, 59-72.

[13] Salathe, E. P., Mathematical studies of capillary tissue exchange, *Bulletin of Mathematical Biology*, 50-3, 1988, 289-311.

[14] Deen, W. M., Robertson, C. R. and Brenner, B. M., Concentration polarization in an ultrafiltering capillary. *BioPhysical Journal*, 14, 1974, 412- 431.

[15] Ross, M. S., A mathematical model of mass transport in a long permeable tube with radial convection, *Journal of Fluid Mechanics,* 63, 1974, 157-175.

[16] Tyagi, V. P. and Abbas. M., An exact analysis for a solute transport, due to simultaneous dialysis and ultrafiltration, in a hollow-fibre artificial kidney, *Bulletin of Mathematical Biology*, 49-3, 1987, 697-717.

[17] Chaturani, P. and Ranganatha, T. R., Solute transfer in fluid in permeable tubes with application to flow in glomerular capillaries, *Acta Mechanica.*, 96, 1993, 139-154.

[18] Varunkumar, M. and Muthu, P., Fluid flow and solute transfer in a tube with variable wall permeability, *Zeitschrift für Naturforschung A-A Journal of Physical Sciences*, 74-12, 2019, 1057-1067.

[19] Varunkumar, M. and Muthu, P., Fluid flow and solute transfer in a permeable tube with influence of slip velocity, *An interdisciplinary journal of Discontinuity, Nonlinearity, and Complexity*, 9-1, 2020, 153-166.
[20] Nazarenko, N. N., The Effect of Barodiffusion on the Distribution of Biological Fluid Velocity and Concentration During Filtration Through a Cylindrical Layer, *Russian Physical Journal*, 63, 2020, 759-764.
[21] Umavathi, J.C., Combined Effect of Variable Viscosity and Variable Thermal Conductivity on Double-Diffusive Convection Flow of a Permeable Fluid in a Vertical Channel, *Transport in Porous Media,* 108, 2015, 659–678.
[22] Awais, M., Bukhari, U., Ali, A., Convective and peristaltic viscous fluid flow with variable viscosity, *Journal of Engineering Thermophysics,* 26, 2017, 69-78.
[23] Davis, R. H. and Sherwood, J. D., A similarity solution for steady-state cross flow microfiltration, *Chemical Engineering Science,* 45, 1990, 3203-3209.
[24] Bowen, W. R. and Williams, P. M., Prediction of the rate of cross-flow ultrafiltration of colloids with concentration-dependent diffusion coefficient and viscosity-theory and experiment, *Chemical Engineering Science*, 56, 2001, 3083-3099.
[25] Shamsuddin, I., Keith, A. S. and Gervas, E. J. M. A., Effect of Viscosity on Membrane Fluxes in Cross-Flow Ultrafiltration, *Separation Science and Technology,* 30(7-9), 1995, 1669-1687.
[26] Pozrikidis. C., Leakage through a permeable capillary tube into a poroelastic tumour interstitium, *Engineering Annals Boundary Elements*, 37, 2013, 728-737.
[27] Pollak, M. R., Susan, E. Q., Melanie. P. H., and Lance. D. D., The glomerulus: The sphere of influence, *Clinical Journal of the American Society of Nephrology* , 9, 2014, 1461-1469.
[9] Misra, J. C., and Ghosh, S. K., A mathematical model for the study of blood flow through a channel with permeable walls, *Acta Mechanica.,* 122, 1997, 137-153.
[28] Shettinger, U. R., Prabhu, H. J. and Ghista. D. N., Blood Ultrafiltration : A Disign Analysis, *Medical and Biological Engineering and Computation.,* 15, 1977, 32-38.

ORCID iD

P Murali Mohan Kumar https://orcid.org/0000-0001-8472-9023
M Varunkumar https://orcid.org/0000-0003-1185-7133